Astron. Astrophys. 239, 142–154 (1990)

ASTRONOMY AND ASTROPHYSICS

Core velocity dispersion and mass-to-light ratio of the old Magellanic globular cluster NGC 1835*

P. Dubath [1,2], G. Meylan **[3,4], M. Mayor [1], and P. Magain [5]

[1] Observatoire de Genève, CH-1290 Sauverny, Switzerland
[2] European Southern Observatory, La Silla, Casilla 19001, Santiago 19, Chile
[3] Space Telescope Science Institute, 3700 San Martin Drive, Baltimore, MD 21218, USA
[4] European Southern Observatory, Karl-Schwarzschild-Strasse 2, D-8046 Garching bei München, Federal Republic of Germany
[5] Institut d'Astrophysique, Université de Liège, Avenue de Cointe 5, B-4200 Cointe-Ougrée, Belgium

Received February 20, accepted May 9, 1990

Abstract. The projected velocity dispersion in the core of the old Large Magellanic Cloud globular cluster NGC 1835 is deduced from integrated light spectra obtained at the European Southern Observatory (ESO) with CASPEC, the Cassegrain ESO Echelle Spectrograph mounted on the ESO 3.6-m telescope at La Silla, Chile. A numerical cross-correlation technique gives a projected velocity dispersion σ_p(core) $= 10.1 \pm 0.2$ km s^{-1}.

Multimass anisotropic King-Michie dynamical models are applied to the observational constraints given by the surface brightness profile and the above central projected velocity dispersion. Depending on the model, the values obtained for the total mass of the cluster range from 0.70 to 1.55 $10^6\,M_\odot$, with a mean total mass $\langle M_{tot}\rangle = 1.0 \pm 0.3\ 10^6\,M_\odot$, corresponding to a global mass-to-light ratio $\langle M/L_V\rangle = 3.4 \pm 1.0\,(M/L_V)_\odot$.

The present study shows that when the same kind of dynamical models (King-Michie) constrained by the same kind of observations (surface brightness profile and central value of the projected velocity dispersion) are applied to an old rich Magellanic globular cluster, viz., NGC 1835, the results seem similar to those obtained in the case of galactic globular clusters. Consequently, the rich old globular clusters in the Magellanic clouds could be quite similar (in mass and M/L_V) to the rich globular clusters in the Galaxy.

Key words: clusters: globular – galaxies : Magellanic clouds – data analysis

1. Introduction

The Large and Small Magellanic clouds (LMC and SMC, respectively), contain a huge potential of astrophysical information. For example, concerning star clusters, the realm of the globular clusters is much richer and varied in the Magellanic clouds than in the Galaxy: rich clusters for all ages are observed, from the youngest, with ages of a few 10^6 yr, to the oldest, with ages of the order or larger than 10 Gyr. In this paper, only old Magellanic and galactic globular clusters are considered, i.e., with ages $\geqq 10$ Gyr.

From the determinations in the literature of the masses of the richest old clusters, a systematic difference seems to exist between the globulars in our Galaxy and in the Magellanic clouds, Magellanic clusters appearing less massive than galactic clusters (e.g., Chun 1978; Kontizas 1984, 1986). Possible dissimilarities in mass and mass-to-light ratio between old rich Magellanic and galactic clusters could reflect systematic differences in the mass function. For example, the brightest old LMC globular cluster, NGC 1835, has a total mass of about 0.1 $10^6\,m_\odot$ corresponding to a M/L_V of about $0.3\,(M/L_V)_\odot$ (mean values from two different methods used by Elson and Freeman 1985), whereas the two brightest galactic globular clusters, ω Centauri and 47 Tucanae, have total masses equal to 3.9 and 1.1 $10^6\,m_\odot$, corresponding to M/L_V equal to 2.9 and 2.1 $(M/L_V)_\odot$, respectively (Meylan 1987, 1989). Such a systematic difference was already discussed, in the case of NGC 1835, by Meylan (1988b), who showed that differences in the methods used to obtain the above parameters can partly explain the discrepancy.

A way to solve this problem consists of obtaining good observational values of the central projected velocity dispersion, by detecting the small Doppler line broadening present in the integrated light spectra because of the spatial random motions of the stars. The central value of the projected velocity dispersion and the surface brightness profile are used for constraining King-Michie dynamical models, allowing a direct comparison with similar studied of galactic globular clusters.

This paper is structured as follows: Sect. 2 enumerates the various methods used until now for obtaining the mass of clusters in the Magellanic Clouds and in the Galaxy and points out the strong dependence of the M/L_V values on the methods used. Section 3 presents and discusses the determination of the projected velocity dispersion in the core of NGC 1835 by a cross-correlation technique applied to the integrated light spectra, Sect. 4 describes the dynamical model, and Sect. 5 displays and discusses the results by using the above velocity dispersion and a composite surface

Send offprint requests to: M. Mayor

* Based on observations collected at the European Southern Observatory, La Silla, Chile

** Affiliated with the Astrophysics Division, Space Science Department, European Space Agency

brightness profile obtained from merging Elson & Freeman (1985), Mateo (1987), and Meylan & Djorgovski (1990) surface brightness profiles. Finally, a summary of this work is given in Sect. 6.

2. Magellanic and galactic M/L_V ratios

2.1. Magellanic globular clusters

The method most often used for obtaining the total mass of Magellanic clusters is related to the systemic rotation of the Magellanic clouds. It is assumed that the clusters are in rotation along circular orbits around the center of mass of the LMC or SMC, the old clusters seeming to form a disk-like subsystem in the case of the LMC (Freeman et al. 1983). In a way similar to the case of galactic open clusters (akin to King 1962), the observed value of the tidal radius r_t of the cluster is transformed into mass according to:

$$M = r_t^3(4\Omega^2 - \kappa^2), \quad (1)$$

where r_t is the cluster tidal radius, and Ω and κ are the rotation angular velocity and the epicyclic frequency, respectively, both at the cluster position (de Vaucouleurs & Freeman 1973; Freeman 1974, 1980; Feitzinger 1980; Prévot et al. 1989). Tidal masses, particularly for the outer clusters, may be underestimated, if these clusters are in radial rather than circular orbits (King 1962).

The observational determination of the tidal radii by star counts in the outer parts of the Magellanic clusters is pioneering work of a difficult nature, since the pollution by Magellanic field stars still induces uncertainties. Determination of tidal radius is a difficult task even for the galactic globular clusters, and the "observed limiting radius" determinations are rather weak for nearly all of them.

Using the above method, Elson & Freeman (1985) found for the old LMC cluster NGC 1835, a total mass equal to $M_{tot} = 7.3\ 10^4\ M_\odot$, with corresponding mean M/L_V ratios equal to $0.18\ (M/L_V)_\odot$.

Reasonably good dynamical constraints – surface brightness profile and central value of the projected velocity dispersion – have been published so far for only one Magellanic cluster: NGC 1835. It is only in the case of this cluster that the determination of the projected velocity dispersion $\sigma_p = 5\,\mathrm{km\,s^{-1}}$, obtained by Elson & Freeman (1985) from a Fourier method applied to integrated light spectra, can be converted into mass (Illingworth 1973), according to:

$$M = 167\, r_c\, \mu\, \sigma_p^2, \quad (2)$$

where r_c is the core radius derived from the fit of the observed surface brightness profile to single-mass isotropic King (1966) models, μ is the dimensionless mass taken from Table II of King (1966), and σ_p is the projected velocity dispersion. Elson & Freeman (1985) find for NGC 1835, $M_{tot} = 1.6\ 10^5\ M_\odot$ with $M/L_V = 0.42\ (M/L_V)_\odot$.

Using the same observational constraints as Elson & Freeman (1985) but applied to multimass anisotropic King-Michie dynamical models, Meylan (1988b) finds a mean total mass of the cluster $\langle M_{tot} \rangle = 3.5 \pm 1.0\ 10^5\ M_\odot$ with a mean mass-to-light ratio $\langle M/L_V \rangle = 1.2 \pm 0.3\ (M/L_V)_\odot$. All the former mass and mass-to-light ratio determinations for NGC 1835 (Freeman 1974; Chun 1978; Elson & Freeman 1985; Meylan 1988b) are displayed in Table 1 and will be discussed in Sect. 5 with the results of the present study.

2.2. Galactic globular clusters

In our Galaxy, only seven globular clusters have been studied so far with King-Michie multi-mass anisotropic dynamical models consisting of about ten different subpopulations. The observational constraints for such models consists in two profiles: first, the surface brightness profile, from surface brightness photometry in the central parts and star counts in the outer regions, second, the projected velocity dispersion profile, from high quality radial velocities of numerous (typically a few hundreds) individual cluster member stars. These seven best studied galactic globular clusters are M3 (Gunn & Griffin 1979), M92 (Lupton et al. 1985), M2 (Pryor et al. 1986), M13 (Lupton et al. 1987), ω Centauri (Meylan 1987), 47 Tucanae (Meylan 1988a, 1989), and NGC 6397 (Meylan & Mayor 1988, 1990). Apart from ω Centauri, the (unique) giant cluster of the Galaxy ($M_{tot} = 3.9\ 10^6\ M_\odot$), the cluster masses range from 0.1 to 1.1 $10^6\ m_\odot$, whereas all the mass-to-light ratios are located between about 2 and 3. The above values can be considered as typical of the masses and mass-to-light ratios of the rich globulars of our Galaxy. They are confirmed by two recent studies of six other galactic clusters, viz., NGC 288, NGC 5466,

Table 1. The different values of the total mass and M/L_V ratio estimates for NGC 1835 published during these last 15 yr

Year	x	M_{tot} [$10^6\ m_\odot$]	M/L_V [$\odot$ units]	r_a [r_c]	Authors
1974	–	0.045	0.2	–	Freeman (1974)
1978	–	0.044	0.12	–	Chun (1978)
1978	–	0.062	0.17	–	Chun (1978)
1985	–	0.073	0.18	–	Elson & Freeman (1985)
1985	–	0.16	0.42	iso	Elson & Freeman (1985)
1988	1.75	0.39	1.30	iso	Meylan (1988b)
1988	1.50	0.28	0.94	30	Meylan (1988b)
1989	1.25	1.03	3.58	iso	Present study
1989	1.00	0.81	2.83	30	Present study

NGC 6624, NGC 6626, NGC 6681, and NGC 6809, studies slightly less constrained by the fact that radial velocities have been obtained for "only" about 20 member stars for each of these clusters (Pryor et al. 1989, 1990).

2.3. *A difference in M/L_V by a factor of 10?*

The typical mass of the rich globular clusters in the Clouds (less than $10^5 M_\odot$) seems smaller than the typical mass of the rich globular clusters in the Galaxy (greater than $10^5 M_\odot$). There are also differences in mass-to-light ratio: $M/L_V \simeq 0.1-0.5\,(M/L_V)_\odot$ for rich clusters in the Magellanic clouds and $M/L_V \simeq 2.0-3.0\,(M/L_V)_\odot$ for the rich clusters in the Galaxy. Is there a genuine systematic difference in M/L_V, by nearly a factor of 10?

It is worth emphasizing that the above question does not only concern globular clusters. For example, despite the range of a factor of 1000 in galaxy luminosities in the Local Group galaxies, the globular cluster luminosity distributions of these galaxies are consistent with being of the same form in all of them (Harris 1987). It is generally accepted that the globular cluster population in galaxies was formed, in all galaxies, with the same distribution of globular cluster masses and luminosities. A clear systematic difference in M/L_V between Magellanic and galactic globular cluster populations would cast doubt as to their use as secondary distance indicators in the cosmological distance ladder.

At the present time, there is no definitive answer. We emphasize that only the rich old globular clusters in the Magellanic clouds and in the Galaxy are considered here. It is essential to realize that any comparison between the M/L_V values of these two populations is so far strongly hampered by the fact that these values proceed from different determination processes. Comparison between galactic and Magellanic M/L_V values should be done only between results coming from the same kind of models constrained by the same kind of observational data. Due to the lack of observational data for the Magellanic clusters, the more elaborate King-Michie dynamical models have been applied so far only to galactic globular clusters (with the exception of NGC 1835, Meylan 1988b).

This situation is on the verge of changing: although it is still difficult to obtain velocity dispersion profiles of Magellanic clusters (Seitzer 1988), it now appears feasable to obtain at least the central value of the projected velocity dispersion, from integrated light spectra. The obtaining of such an essential observational constraint, in the case of the old Magellanic globular NGC 1835, is presented below, with a discussion of the application of this new result to a King-Michie model and the consequences on the M/L_V ratio of this cluster.

3. Core velocity dispersion from cross-correlation technique

3.1. *Optical and numerical cross-correlations*

For more than twenty years, cross-correlation spectroscopy has proven its exceptional efficiency in radial velocity determination, thanks to the pioneering work of Griffin (1967). The cross-correlation between a stellar spectrum and a template allows the radial velocity information contained in the stellar spectrum to be condensed into the equivalent of a single spectral "line": the cross-correlation function. For example, with the two CORAVEL spectrometers (Baranne et al. 1979) mounted on 1-m class telescopes, using simultaneously about 1500 spectral lines, a few minutes of integration provide a determination of the radial velocity of a 14th V-magnitude star with a precision of about $1\,\mathrm{km\,s^{-1}}$.

In such spectrometers, the cross-correlation is done optically, but it is easy to visualize obtaining the same result from a numerical correlation between spectra registered on CCD. Such radial velocity measurements are nowadays routinely obtained, e.g., by Latham (1985) and his collaborators from numerical cross-correlation of registered Reticon spectra having a wavelength range of 50 Å. A similar numerical cross-correlation, using spectra taken with CASPEC, the Cassegrain Echelle Spectrograph of the European Southern Observatory (ESO) mounted on the ESO 3.6-m telescope at La Silla, Chile, would take advantage of a much larger spectral range (larger than 1000 Å). The numerical cross-correlation gives a priori a noticeable advantage: the scanning required to build optically the CORAVEL cross-correlation function on the telescope is no longer necessary, providing an immediate gain of about 2.5 mag. In addition, we can expect some further gain due to the high quantum efficiency of CCDs as compared to photomultipliers. Unfortunately the read-out noise of the CCDs is still a limiting factor.

If the cross-correlation spectroscopy is well adapted to radial velocity determinations, it shows the same efficiency concerning line broadening measurements, giving access to rotation through precise $V \sin i$ (Benz & Mayor 1981, 1984). The cross-correlation function of the integrated light spectra of globular cluster cores should allow a determination of the projected velocity dispersion of the stars in these cores. A resolution of about 20000 is needed to have access through cross-correlation spectroscopy to Doppler broadenings of a few $\mathrm{km\,s^{-1}}$, but a low signal-to-noise ratio, as low as 2–3, is admissible. A similar approach was already used by Illingworth (1976) to determine the projected velocity dispersion in the nucleus of some galactic globular clusters, using Fourier transforms of integrated light spectra on photographic plates. Recently, projected velocity dispersion in the core of M15 has been obtained from cross-correlation technique applied to CCD long-slit spectra (Peterson et al. 1989).

3.2. *Observations*

In order to investigate the possibilities of CASPEC spectra applied to this technique, we obtained two hours of test time at the ESO 3.6-m telescope, during the night 11–12 Nov 1987. The ESO CCD No. 3 was used for all these observations. It is an RCA SID 501 EX thinned, backside illuminated device, with 320×512 pixels of 30 μm square, and with a readout noise of about 40 electrons. This instrument was used in a normal setup, with the 31.6 line $\mathrm{mm^{-1}}$ grating and with a wavelength domain between 4400 and 5500 Å, centered on the maximum of sensitivity of the CCD. The seeing values obtained at the ESO 2.2-m telescope during the time of our observations (at about 2–4 UT) were typically of the order of 1″.2. The dimensions of the entrance slit, 1″.2 × 6″.0, were the same for all the observations. Spectra of a thorium lamp were obtained before and after every astronomical spectra, with the telescope pointing towards the cluster or standard star observed. During the exposures of the globular clusters, a scanning of the nucleus was done with the entrance slit, in order to cover a zone of 6″ × 6″, for avoiding any problem of sampling which could occur if integrating only over a few bright stars. For illustrative purpose, this sampling area is represented in Fig. 1 by a 6 arcsec square centered on the core of NGC 1835; this CCD frame is the result of a 3 min exposure obtained at La Silla with the ESO 2.2-m telescope, on 18 Dec 1987 with a V Bessel filter (Meylan & Djorgovski 1990). Spectra were obtained for two old

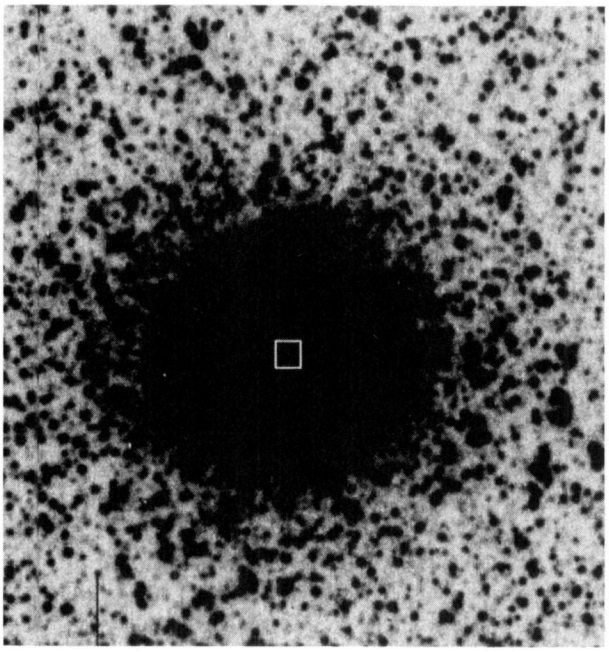

Fig. 1. NGC 1835: this CCD frame has been obtained at the European Southern Observatory, La Silla, Chile, with the ESO 2.2-m telescope, on 18 Dec 1987 with a V Bessel filter. The central white square, $6'' \times 6''$, corresponds to the sampling region over which the integrated light spectra have been obtained

globular cluster nuclei of the Large Magellanic Cloud and for two K 5 III comparison stars. The integration time is 30 min for each of the two exposures for NGC 1835, and 20 min for each of the two exposures for NGC 1978. Only results concerning NGC 1835 are discussed in the present study.

All these spectra were reduced following standard procedures. The CCD frames were first cleaned to remove bad areas and median filtered to remove the cosmic events. The backgrounds were then subtracted, and the different orders extracted, wavelength calibrated (by using Thorium-Argon spectra), normalized and finally merged together. Unnormalized spectra were also used during the cross-correlations analysis. Any flux calibration being useless when cross-correlating spectra for obtaining radial velocity or projected velocity dispersion, no flat field operation was applied. All these operations were achieved using the ESO MIDAS package on the VAX 780 computer at Geneva Observatory.

In the left half of Fig. 2, 100 Å ranges from the normalized spectra of one comparison star (HD 31871, K 5 III, $m_V = 9$) and of the two clusters NGC 1835 and NGC 1978 are displayed. Due to the large difference in central surface brightness between the two clusters, the signal-to-noise ratio of the two cluster spectra are quite different. The case of NGC 1978 is especially interesting for illustrating the potentialities of the method: the spectrum of this cluster has only a signal-to-noise ratio of about 2 (NGC 1978 will be the subject of another paper).

3.3. *Numerical cross-correlation*

The new software developed here for numerical cross-correlation technique mimics CORAVEL: it reproduces numerically with registered spectra what is achieved optically online at the telescope with CORAVEL. For the sake of this goal, the numerical version of the CORAVEL mask has been used here as a template. This mask is built from the spectrum of Arcturus (Griffin 1968); its conception and its optimization are well described in Baranne et al. (1979). For most Arcturus spectral lines, the mask provides two values: the lower and upper limits of a wavelength window, centered on the line and of optimized width. For any radial velocity, i.e., for any shift in wavelength between the registered spectrum and the mask, a point of the correlation function is evaluated by calculating the integral of the spectrum considered through the mask windows (the cross-correlation function is a simple integral because the template is a binary function). The whole cross-correlation function is constructed by evaluating the integral for as many shifts as desired. In the present case, every shift corresponds to $1\,\mathrm{km\,s^{-1}}$. Beginning with the lowest chosen radial velocity and carrying on the computation by steps of $1\,\mathrm{km\,s^{-1}}$ towards the highest chosen radial velocity, the correlation function is built step by step while the whole chosen velocity domain is covered. With such a way of achieving the correlation, one can clearly realize the meaning of the *correlation function:* it is a kind of "average spectral line" over all the lines present in the template. It is worth mentioning that strong saturated lines which contain little or no information about the radial velocity have been excluded, consequently, as in the case of the CORAVEL mask, only small unsaturated lines have been used to build the numerical mask used here (Baranne et al. 1979). In order to take advantage of our experience with CORAVEL, only the spectral domain common to the CORAVEL mask (3600–5200 Å) and to the present CASPEC spectra (4400–5200 Å) has been used, viz., the interval from 4400 to 5200 Å.

In the right half of Fig. 2, the cross-correlation functions obtained for one comparison star and for the clusters are displayed (only for illustration purpose in the case of NGC 1978). The correlation functions, as for those obtained with CORAVEL spectrometers, are very close to gaussians, consequently gaussian fits are very satifactory and deliver the parameters of the correlation functions, i.e., the position in radial velocity, the value of the continuum (which has been normalized to one in Fig. 2), and the depth and the width of the dip. Due to their low metallicities, the cross-correlation functions of the two clusters are much less contrasted than the cross-correlation functions of the two comparison stars. As the present numerical technique is similar to the online technique of CORAVEL spectrometers, the present numerical cross-correlation functions do have the same behavior as the CORAVEL cross-correlation functions. For example, CORAVEL experience shows that the width of the cross-correlation function does not depend on the metallicity. Therefore, the broadening of these clusters cross-correlation functions are only produced by the Doppler line broadening present in the integrated light spectra because of the spatial random motions of the stars.

After normalization of the cross-correlation function of the cluster NGC 1835, in order to have the same depth as the cross-correlation function of the comparison star, we immediately notice the important broadening of the cluster cross-correlation function (Fig. 3). Both comparison stars have been checked by direct CORAVEL measurements to have an almost zero rotation. Consequently, the projected velocity dispersion in the core of NGC 1835 is immediately derived:

$$\sigma_p\,(\mathrm{core}) = 10.1 \pm 0.2\,\mathrm{km\,s^{-1}}\,.$$

A discussion about the uncertainties in this projected velocity dispersion measurement is given in Sects. 3.4 and 3.5 below. It is

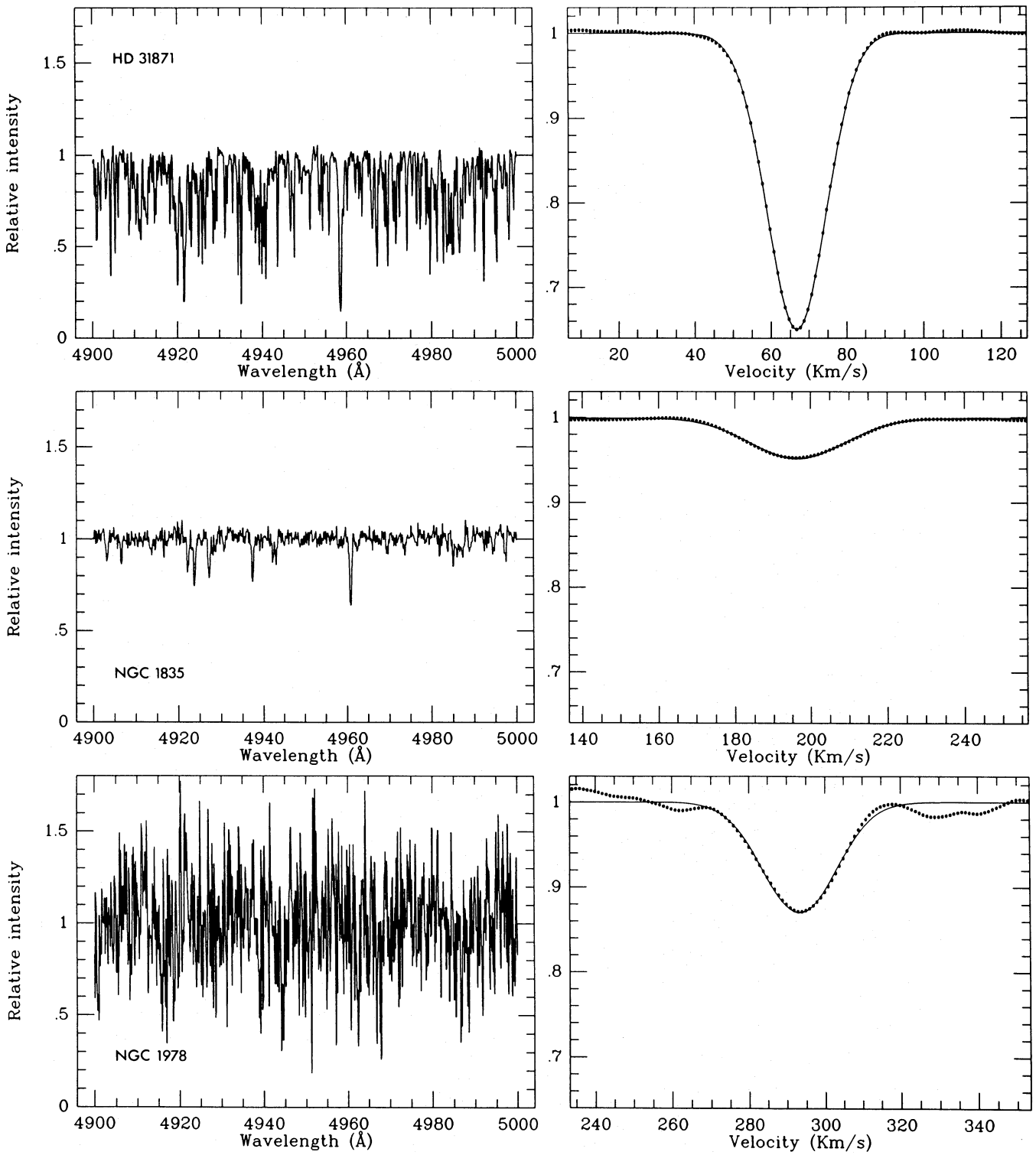

Fig. 2. *Left:* for the comparison star HD 31871 (K 5 III, $m_V = 9$), and for the two old LMC globular clusters NGC 1835 and NGC 1978, 100 Å ranges are displayed for each spectra obtained with CASPEC (Cassegrain ESO Echelle Spectrograph mounted on the ESO 3.6-m telescope at La Silla). *Right:* numerical cross-correlation functions for the same three objects; the cross-correlation functions of the two clusters, because of low metallicities, are much less contrasted than the cross-correlation function of the comparison star. CORAVEL experience shows that the width of the cross-correlation function does not depend on the metallicity

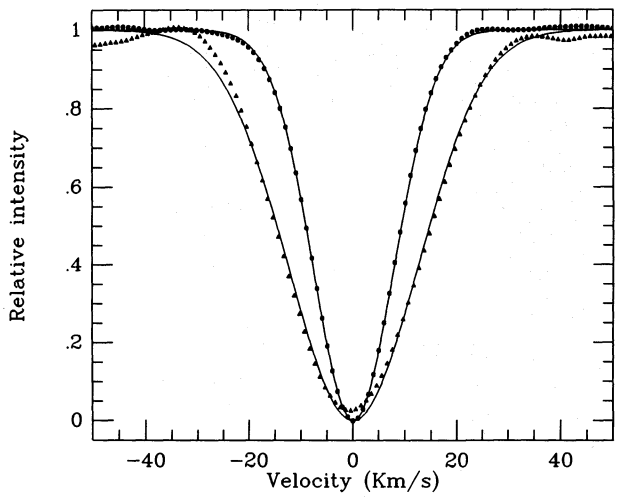

Fig. 3. Normalized cross-correlation functions of the cluster NGC 1835 (triangles) and of the comparison star HD 31871 (dots); the continuous lines are the corresponding fitted gaussians; the important broadening of the cluster cross-correlation function is conspicuous and allows an immediate determination of the projected velocity dispersion in the core of NGC 1835: $\sigma_p = 10.1 \pm 0.2\,\mathrm{km\,s^{-1}}$

worth mentioning here that the cross-correlation technique allows us to determine accurately a broadening of only a few percent of the FWHM of the cross-correlation function (at zero broadening factor, the FWHM of the CASPEC cross-correlation function is equivalent to about $18\,\mathrm{km\,s^{-1}}$, the pixel size being $9\,\mathrm{km\,s^{-1}}$).

Normalized spectra have been used in the cross-correlation process, but investigation by using unnormalized spectra produce no significant differences on the results. The unnormalized spectra show, first, oscillations (one per order, as the central part of the orders receive more light than the extremities) and, second, a slow increase of the continuum from the blue to the red (because of the CASPEC sensitivity and the cluster spectrum continuum). The oscillations have too low a frequency to degrade the cross-correlation function. However, the effect of the spectral continuum slope could be to incline slightly the cross-correlation function continuum: such an effect is not observed in the present study.

The continuum of the cross-correlation function obtained with the unnormalized spectra gives a measure of the average of the continuum over the whole spectrum. Knowing the transmission of the template (i.e., the total pixel number integrated to get one point of the cross-correlation function), this leads to an estimate of the average signal value per pixel. The noise on our "average pixel signal" can be computed, since it is, in first approximation, the square root of the quadratic sum of (i) the photon counting noise (given here by the square root of our average signal value per pixel) and (ii) the readout noise. Both noises are given in electron or photon units. Average signal-to-noise ratios for the whole spectra are derived for each observed astronomical targets: S/N = 82 for HD 31871 and S/N = 52 for HD 43880, the two standard stars; S/N = 18 for NGC 1835 and S/N = 1.3 for NGC 1978.

3.4. Numerical simulations concerning error estimates

In order to estimate the influences of both photon counting and readout noises on the present determinations of radial velocity V_r and projected velocity dispersion σ_p, the following numerical simulations have been carried out.

First, we consider the original CCD frame, with relatively high S/N ratio (S/N = 82), of the standard star HD 31871 (part of its spectrum is displayed in Fig. 2). To simulate the case of a spectrum with weaker spectral lines (as in the case of a low metallicity object), suitable constants are added to this frame in order to obtain, after reduction and cross-correlation with the template, cross-correlation functions of smaller relative depths. Four additive constants are used, which lead to four frames with still relatively high S/N ratios, and which give cross-correlation functions with relative depths equal to 0.1, 0.2, 0.3, and 0.4.

Second, some frames with known gaussian noises are generated and added to the above four frames to degrade their S/N ratios in order to simulate the photon counting and readout noises of real low S/N images. Four different standard deviations are chosen for the gaussian frames, corresponding to signal-to-noise ratios of 1, 2, 3, and 4 for the extracted spectra. For the computation of these S/N ratios, the signals S are given a posteriori by the average signal value per pixel from the continuum of the respective cross-correlation function, and the noises N are the standard deviations of the gaussian frames (the noise of the original spectrum of HD 31871 is negligible).

Consequently, there are 16 different combinations of cross-correlation function depths and S/N values (4 depths, and 4 S/N ratios). For each of these 16 cases, 120 simulations are carried out (i.e., generation of a gaussian frame, addition of this frame to one of the nearly noiseless frames, complete reduction, and cross-correlation).

The standard deviations ε of the radial velocities resulting from these simulations are displayed in Fig. 4a, as a function of the relative depths of the cross-correlation dips. Each point represents the 120 simulations concerning one of the 16 cases. The cases corresponding to S/N ratios equal to 1, 2, 3, and 4 are represented by pentagons, triangles, squares, and filled circles, respectively. The point corresponding to the values (Depth, S/N) = (0.1, 1) is out of the figure (upper left corner), with $\varepsilon = 3.5\,\mathrm{km\,s^{-1}}$. The standard deviations ε of the widths (FWHM) of the cross-correlation dips, resulting from the same above simulations, are displayed in Fig. 4b, as a function of the relative depths of the cross-correlation dips (the same symbols are used). The point corresponding to the values (Depth, S/N) = (0.1, 1) is again out of the figure (upper left corner), with $\varepsilon = 4.7\,\mathrm{km\,s^{-1}}$.

The relative depths of the cross-correlation dips are, for the noiseless cases, equal to 0.1, 0.2, 0.3, and 0.4. It is noticeable on Fig. 4a and b that a larger noise reduces this depth. This effect is the most significant for S/N ratios equal to one (pentagons), however this effect is small already with S/N ratios equal to four (filled circles). In both figures the relative errors on the standard deviations ε (in $\mathrm{km\,s^{-1}}$) are equal to 6.5%, and are represented by the error bars; the errors on the depth of the cross-correlation dips are smaller than the symbols used.

The following formula,

$$\varepsilon = \frac{C}{(\mathrm{S/N})\,D}, \tag{3}$$

where C is a constant, S/N is the signal to noise ratio, and D is the depth of the cross-correlation dip, is fitted to each of the different groups of points. The results are represented by the continuous lines in both Fig. 4a and b. The constant equals $C = 0.204 \pm 0.012$, and $C = 0.189 \pm 0.011$ for the radial velocities (Fig. 4a) and the widths (Fig. 4b), respectively. Consequently, a mean value equal to $C = 0.2$ is valid in both cases. Equation (3) gives an estimate of the uncertainty ε on the radial velocity and on the projected

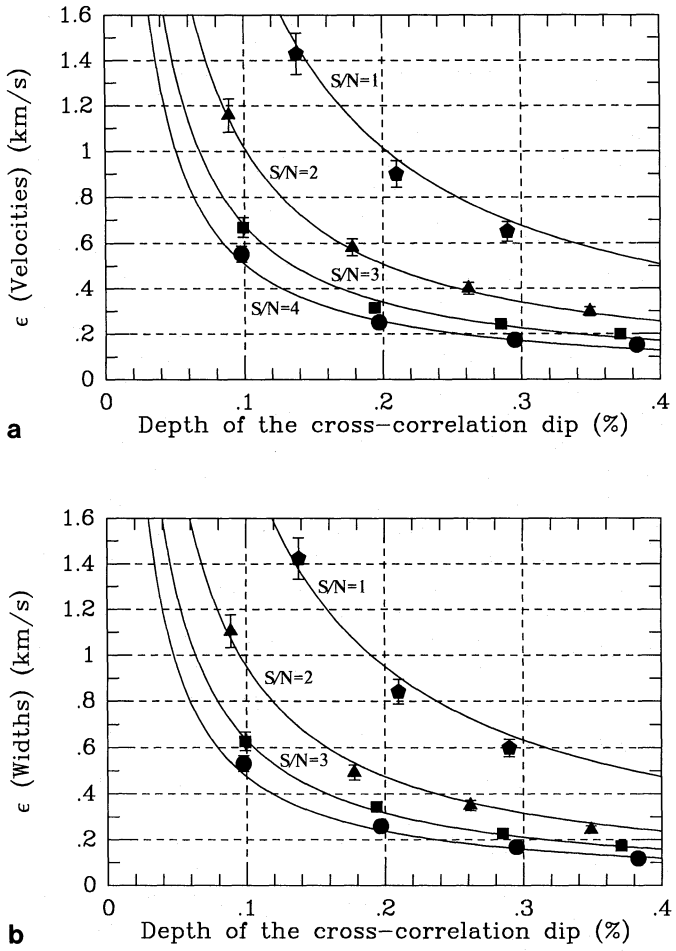

Fig. 4a and b. Results of the numerical simulations concerning the estimate of the uncertainty ε due to photon counting and readout noises. In **a** (top), ε represents the standard deviation of the radial velocities; in **b** (bottom), ε represents the standard deviation of the widths (FWHM) of the cross-correlation dips. Values of ε (km s^{-1}), as a function of the relative depth of the cross-correlation dip, are given for four different values of the S/N ratio (S/N = 1, 2, 3, and 4, corresponding to pentagons, triangles, squares and filled circles, respectively). Each point represents the standard deviation from the results of 120 simulations. The points corresponding to the values (depth, S/N) = (0.1, 1) are out of the figure (upper left corner). The continuous lines are the results of fits with the formula given by Eq. (3)

velocity dispersion, due to photon counting and readout noises, as a function of the signal-to-noise ratio S/N of the considered spectrum, and as a function of the depth D of the corresponding cross-correlation function dip.

In the case of NGC 1835, with S/N = 18 and $D = 0.05$, the uncertainty ε on the projected velocity dispersion is about 0.2 km s^{-1}. Therefore, from a technical point of view, the present work is probably not limited by the photon counting and readout noises, but rather by the intrinsic accuracy of the CASPEC spectrograph attached to the ESO 3.6-m telescope. Further observations of a complete sample of radial velocity standard stars are needed to investigate more widely the accuracy of the present technique. From the resolving power of CASPEC – about 20000 – and from comparison of the present standard star velocities with their CORAVEL measurements, estimates of the uncertainty on the projected velocity dispersion give values smaller than 1 km s^{-1}.

3.5. Possible sources of error

The fact that the present new determination of the projected velocity dispersion in the core of NGC 1835, viz., σ_p(core) = 10.1 ± 0.2 km s^{-1}, is significantly larger than the only previous determination concerning this cluster, viz., σ_p(core) = 5 km s^{-1}, obtained by Elson and Freeman (1985), calls for some comments. Seitzer (1990) has measured radial velocities for 8 stars inside 30″ from the core of NGC 1835, by using echelle spectra obtained with the 4-m telescope at the Cerro Tololo Interamerican Observatory, Chile. The mean accuracy of each radial velocity is 1.5 km s^{-1}. The projected velocity dispersion equals $\sigma_p(\leqq 30'') = 6.8 \pm 1.5$ km s^{-1}. Considering the fact that the velocity dispersion profiles of the already studied galactic globular clusters increase from 30″ towards the inner core, the value of 10.1 km s^{-1} for the core projected velocity dispersion is consistent with the more external value of 6.8 km s^{-1}. It is worth noticing that the present value corresponds to a square of 6″ centered on the cluster core. The dimensions of the sampling area used by Elson & Freeman (1985), not given in their paper, is perhaps larger, in which case it would explain their 5 km s^{-1}, a lower value because averaged over a larger area.

The above discussion (Sect. 3.4) about numerical simulations concerns only internal error associated with the present numerical cross-correlation technique. Apart from the consistency of our result with Seitzer's projected velocity dispersion determination, it is worth investigating the possible sources of external errors in our method.

(i) Telescope flexions, poor calibration: this kind of problem has been prevented by a careful sequence of observations, with lamp calibration spectra taken immediately before and after every cluster and standard observations. Comparisons of the results concerning the standards with previous observations show close agreements.

(ii) Rotation of the cluster: the conclusion of the present work (Sect. 6 below) consists in the fact that NGC 1835 looks similar to 47 Tuc. In particular, these two clusters have similar concentration. Investigations concerning the influence of the rotation can be based on the assumption that NGC 1835 has a rotation similar to the one observed in 47 Tuc, in which the maximum of the rotation curve peaks at $12 r_c$, corresponding to 6–7 pc. Consequently the rotation curve in NGC 1835 (not detected yet) could peak at the same distance from the center of the cluster, i.e., at $12 r_c$ corresponding to 33″. The sampling area of 6″ × 6″, corresponds here to a distance of $3'' \simeq 1 r_c$, a distance inside of which the rotation of 47 Tuc is negligible (smaller than 1 km s^{-1}). Then, the rotational component of the observed line broadening in the cluster is expected to be negligible.

(iii) Number of stars sampled: once again, similarly to 47 Tuc, the central density of NGC 1835 can be considered to be $\varrho_0 \simeq 10^4 M_\odot$ pc^{-3} (Table 3). Even if less than 1% of this mass is under the form of stars with individual masses between 0.63 and 0.90 $M_\odot$, the total number of giant stars being inside a square of 6″ (corresponding to a side of $\sim 2 r_c$) amounts to a few hundreds. There is no danger, in the present measurements, of sampling only over a few bright stars.

(iv) Metallicity effect: the two comparison stars, with spectral type K5 III, clearly have much larger metallicities than NGC 1835. However, the width of the cross-correlation function, based on the CORAVEL template, is completely insensitive to metallicity. From the measurements obtained with the two existing CORAVEL spectrometers, the observed lower limits of

the cross-correlation function widths ($V \sin i = 0$) are identical for both population I and II stars.

(v) Stellar rotation and macroturbulence: from a recent extensive study of about one thousand giant stars observed with CORAVEL, it appears that the $V \sin i$ of K giants are extremely small: the mean rotation of such stars is about $1\,\mathrm{km\,s^{-1}}$ (de Medeiros & Mayor 1990). CORAVEL measurements of giant stars, members of globular clusters, do not display any detectable stellar rotation. The difference in macroturbulence between K giants of populations I and II is not detected either.

(vi) Field contamination: NGC 1835 being close to the bar of the LMC, the pollution from field stars is important in the outer region of the cluster. Nevertheless, right in the core, i.e., where the present observations are made, the density of cluster stars overwhelms the density of field stars: the pollution in negligible.

4. The present model

4.1. The mass function

Because the mass function is still unknown, and in order to mimic a real cluster, main sequence (MS) stars, white dwarfs, and heavy remnants (such as stellar black holes and/or neutron stars), are distributed into ten different mass classes, adopting the following power-law form for the initial mass function (IMF):

$$\mathrm{d}N \propto m^{-x}\,\mathrm{d}\log(m), \tag{4}$$

where the exponent x would equal 1.35 in the case of Salpeter's (1955) galactic IMF.

This mass function must be cutoff at both extremities. The upper limit has no dynamical or photometric influence, because it concerns only small numbers of stars that have already evolved into heavy remnants: e.g., for $x = 1.5$, the fraction of the total mass in the form of heavy remnants varies by 0.05% when going from an upper limit of 150 to 50 $M_\odot$; for $x = 1.0$, the same fraction varies by 0.6%, and for $x = 0.5$, by 4.0%. Since the fraction of the total mass in the form of heavy remnants is itself always less than 5%, the above variations are much smaller than the uncertainty on the total mass. The upper limit is chosen rather arbitrarily at 100 $M_\odot$. The lower limit is much more controversial because of the potential dynamical importance of a large number of low luminosity stars. But in any case we notice, as Gunn & Griffin (1979) found, that this lower mass cutoff, if it is low enough, does not significantly affect the cluster structure as traced by the giant stars. It does not influence the quality of the fit, but only the total mass of the cluster. The individual mass of the lightest stars is taken equal to $0.13\,M_\odot$; investigation with slightly different cutoffs does not influence the conclusions of this work. Owing to the total lack of observation concerning variations in the mass function along the MS, the exponent x is taken the same for the whole range in mass.

NGC 1835 being slightly younger than the galactic globular clusters, the turnoff mass for this cluster is slightly larger than the common value for galactic globulars ($m_{\mathrm{to}} \simeq 0.8\,M_\odot$). Adopting an age of 10 Gyr for NGC 1835 (Elson & Freeman 1985), we take the turnoff mass equal to $m_{\mathrm{to}} = 0.9\,M_\odot$(Renzini & Buzzoni 1986). A variation of m_{to} by $0.2\,M_\odot$ does not change the general conclusions of the present work. The MS stars are binned in 8 mass classes, between $m = 0.9$ and $0.13\,M_\odot$. Thus all stars with initial mass m_{init} lighter than $0.9\,M_\odot$ are still on the MS, unlike all the heavier stars, which have already evolved. The ultimate fate of these stars is treated in the following manner:

1) Stars with initial mass $m_{\mathrm{i}} \in [5, 100]\,M_\odot$ are supposed to end as heavy remnants (hereafter hr) in the form of black holes and/or neutron stars, with mean individual mass $m_{\mathrm{hr}} = 2.0$ or $1.4\,M_\odot$, respectively (each model using one of these two values in turn).

2) Stars with initial mass $m_{\mathrm{i}} \in [2.5, 5]\,M_\odot$ are supposed to end in the form of heavy white dwarfs with a final mass $m_{\mathrm{wd}} \simeq 1.1\,M_\odot$.

3) Stars with initial mass $m_{\mathrm{i}} \in [1.5, 2.5]\,M_\odot$ are supposed to end in the form of intermediate mass white dwarfs with a final mass $m_{\mathrm{wd}} \simeq 0.75\,M_\odot$; these remnants are dynamically mixed into the bin of MS stars having $m_{\mathrm{i}} \in [0.63, 0.9]\,M_\odot$.

4) Stars with initial mass $m_{\mathrm{i}} \in [0.9, 1.5]\,M_\odot$ are supposed to end in the form of light white dwarfs with a final mass $m_{\mathrm{wd}} \simeq 0.58\,M_\odot$; these remnants are dynamically mixed into the bin of MS stars having $m_{\mathrm{i}} \in [0.50, 0.63]\,M_\odot$.

The division of the white dwarfs into the 3 above subpopulations (see e.g., Meylan 1987 for details) is done by using a formula from Iben & Renzini (1983), which gives results in good agreement with the observational frequencies of the individual masses of white dwarfs (Weidemann & Koester 1983; Guseinov et al. 1983; Weidemann 1987).

4.2. Basic equation of the model

A King-Michie dynamical model based on an assumed form for the phase-space distribution function, has been constructed in an approach nearly identical to that of Gunn & Griffin (1979). Each of the 10 subpopulations used has an energy-angular momentum distribution function (Michie 1963, King 1966) given by:

$$f_i(E, J) \propto [\exp(-A_i E) - 1]\exp(-\beta J^2). \tag{5}$$

The model is spherical with radial anisotropy of the velocity dispersion, but has no rotation. Because of the short relaxation time expected in the cluster center, thermodynamic equilibrium is assumed in order to force A_i to be proportional to the mean mass $\bar{m}_i$ of the stars in the subpopulation considered (see discussed Sect. 5.3).

By adopting a scale radius r_{c} and a scale velocity v_{s}, Eq. (5) transforms, in dimensionless quantities, into:

$$\bar{f}_i(\xi, u) = \alpha_i C_i \exp\left(-\frac{1}{2}\mu_i u_\perp^2\,\xi^2\,\xi_t^2\right)\left[\exp\left(-\frac{1}{2}\mu_i u^2 + \mu_i W\right) - 1\right], \tag{6}$$

where $\alpha_i = \varrho_{0,i}/\varrho$ is the fractional density contribution of mass class i at the center, C_i a normalization constant related to the definition of the dimensionless density $\sigma_i = \varrho_i/\varrho_0$, $\mu_i = m_i/\bar{m}$ the normalized mean individual mass of a star of class i, $u = v/v_s$ (with $u_\perp$ the tangential component) the dimensionless velocity, $\xi = r/r_{\mathrm{c}}$ the dimensionless radius, and $W = -\Psi/v_{\mathrm{s}}^2$ the dimensionless potential [for more details the reader is referred to the original paper of Gunn & Griffin (1979), and to Meylan (1987, 1988a, and 1989) for application to ω Centauri and 47 Tucanae, respectively].

A model is specified by a mass function exponent x, used in Eq. (4), and by four parameters: (i) the scale radius r_{c}, (ii) the scale velocity v_{s}, (iii) the central value of the gravitational potential W_0, and (iv) the anisotropy radius r_{a}. Beyond the anisotropy radius, the velocity dispersion tensor becomes increasingly radial.

For each model, two "average" relaxation times are obtained: a half-mass relaxation time and a central relaxation time. The term "average" comes from the fact that they depend on the mean stellar mass of the system, instead of being related to one particular species. The standard formula (Spitzer & Hart 1971) transforms into:

$$t_{\rm rh} = (8.92\ 10^5\ {\rm yr})\ \frac{(M/1\,m_\odot)^{1/2}}{(\bar{m}/1\,m_\odot)}\ \frac{(r_{\rm h}/1\ {\rm pc})^{3/2}}{\log\,(0.4\,M/\bar{m})}, \qquad (7)$$

where M is the total mass of the cluster, $r_{\rm h}$ the half-mass radius, and $\bar{m}$ the mean stellar mass of all the stars in the cluster. The central value of the relaxation time is given by (e.g., Lightman & Shapiro 1978):

$$t_{\rm r,0} = (1.55\ 10^7\ {\rm yr})\ \frac{(1\,m_\odot/\bar{m}_0)}{\log\,(0.5\,M/\bar{m})}\ \frac{v_{\rm s}}{1\ {\rm km/s}}\left(\frac{r_{\rm c}}{1\ {\rm pc}}\right)^2, \qquad (8)$$

where $\bar{m}_0$ is the mean mass of all the particles in thermodynamic equilibrium in the central parts, $v_{\rm s}$ the velocity scale, and $r_{\rm c}$ the scale radius.

4.3. The fit to the observational constraints

Ideally, King-Michie dynamical models are constrained by comparing, first, the observed and model surface brightness profiles, and second, the observed and model velocity dispersion profiles.

The observed surface brightness profile is a composite profile – namely CCD surface brightness photometry in the core and the inner parts, centered aperture photometry and drift scan measures in the central and intermediate parts, and star counts in the outer parts – obtained by mixing Elson & Freeman (1985), Mateo (1987), and Meylan & Djorgovski (1990) data. The composite profile obtained (68 points) is displayed numerically in Table 2, where the first column gives the index of the points, the second column gives the logarithm of the radius in arcsec, the third column gives the surface brightness in V mag arcsec^{-2}, and the fourth column indicates the source in the literature. In order to avoid giving precedence, during the fitting procedure, to any of the three observational sources, the same arbitrary uncertainty, equal to 0.100 V mag arcsec^{-2}, is used for all points.

The other observational constraint, the projected velocity dispersion profile, is unfortunately reduced to one point, viz., the central value. This fact prevents a real comparison of the shapes of the observed and model projected velocity dispersion profiles, shape related to the quantity of anisotropy, but it allows

Table 2. NGC 1835: composite surface brightness profile from: (1) Elson & Freeman (1985), (2) Mateo (1987), and (3) Meylan & Djorgovski (1990)

No.	log r [arcsec]	Σ_V [V mag arcsec^{-2}]	Ref.
1	−0.523	15.706	3
2	−0.456	15.565	2
3	−0.310	15.672	3
4	−0.222	15.650	3
5	−0.201	15.618	2
6	−0.131	15.668	3
7	−0.056	15.653	2
8	−0.046	15.629	3
9	0.041	15.642	3
10	0.100	15.745	2
11	0.130	15.758	3
12	0.217	15.817	3
13	0.243	15.891	2
14	0.303	15.964	3
15	0.391	16.110	3
16	0.401	16.108	2
17	0.477	16.268	3
18	0.544	16.399	2
19	0.565	16.471	3
20	0.652	16.735	3
21	0.703	16.889	2
22	0.739	17.097	3
23	0.826	17.372	3
24	0.845	17.376	2
25	0.913	17.627	3
26	1.000	18.103	3
27	1.004	18.052	2
28	1.037	18.250	1
29	1.087	18.500	3
30	1.099	18.510	1
31	1.129	18.655	2
32	1.153	18.830	1
33	1.174	18.914	3
34	1.200	19.060	1

Table 2 (continued)

No.	log r [arcsec]	Σ_V [V mag arcsec^{-2}]	Ref.
35	1.208	19.172	2
36	1.261	19.437	3
37	1.270	19.517	2
38	1.328	19.720	1
39	1.348	19.722	3
40	1.350	19.782	2
41	1.435	20.240	3
42	1.437	20.426	2
43	1.438	20.470	1
44	1.509	20.906	2
45	1.522	20.674	3
46	1.539	20.870	1
47	1.571	21.063	2
48	1.572	21.100	1
49	1.622	21.380	1
50	1.625	21.455	2
51	1.655	21.580	1
52	1.673	22.199	2
53	1.685	21.850	1
54	1.716	21.963	2
55	1.729	22.080	1
56	1.753	22.570	1
57	1.756	22.412	2
58	1.792	22.587	2
59	1.816	22.890	1
60	1.825	22.355	2
61	1.860	23.140	1
62	1.923	23.880	1
63	1.953	24.830	1
64	1.961	24.090	1
65	1.968	24.620	1
66	1.994	24.840	1
67	2.024	25.370	1
68	2.051	26.060	1

nevertheless the estimate of the total mass of the cluster. We use our new determination for the projected velocity dispersion in the core of NGC 1835: $\sigma_p(\text{core}) = 10.1 \pm 0.2\,\text{km s}^{-1}$.

The stars contributing most of the light are heavier than $0.63\,M_\odot$. Consequently the fits between the models and the observations are made by using the projected surface brightness and velocity dispersion profiles of only one population, which contains giants, subgiants, turnoff stars, and stars at the top of the MS, i.e., the brightest members in the cluster, dynamically mixed with the intermediate-mass white dwarfs.

In order to compare our results with the previous mass determinations, the distance modulus of the LMC used by all the other authors (Freeman 1974; Chun 1978; Elson & Freeman 1985) is adopted, $(m-M)_0 = 18.7$, which corresponds to a distance to the LMC of 55 kpc.

5. The results

5.1. Generalities

Tables 3 and 4 display some results concerning only the 6 best models (lowest reduced χ^2_ν) from a grid of about 500 models. The model with index 4a, isotropic as model 4, is calculated with a partial thermalization (see Sect. 5.3 below). The model with the index 5a differs from the model 5 only by the central value of the projected velocity dispersion, taken equal to $11.1\,\text{km s}^{-1}$ in model 5a instead of $10.1\,\text{km s}^{-1}$ in model 5; the model with the index 5b differs from model 5 only by the distance modulus, taken equal to 18.2 (e.g., Andersen et al. 1985) in model 5b instead of 18.7 in model 5 (see Sect. 5.3 below).

Figure 5 displays the observed surface brightness profile (68 points), as a function of the radius, fitted to the computed surface brightness profile of the model with index 1 in Tables 3 and 4. The model profile, integrated along the line-of-sight, concerns only the population with index 3 (see Sects. 4.1 and 4.3). The residuals between observations (points) and model (continuous line) are also displayed in the lower part of the same figure.

5.2. Mass function exponent, total mass, and mass-to-light ratio

The models are calculated by using the same mass function exponent $x\,(\text{d}N \propto m^{-x}\,\text{d}\log(m))$ for the entire range in stellar mass, i.e., from 0.1 to 100 $M_\odot$. Within the large range of values of x investigated (from 0.0 to 3.5 by steps of 0.25), only the values between 1.00 and 1.75 provide models able to fit the observations. Only models with small fractions of stellar remnants (neutron stars and white dwarfs) fit the observations: the fraction of the total mass in the form of neutron stars varies from 0.0 to 4%, whereas the fraction of the total mass in the form of white dwarfs varies from 9 to 26%, depending on the model.

From a structural point of view, NGC 1835 appears rather concentrated, with values of the concentration parameter $c = \log(r_t/r_c)$ ranging from 1.81 to 2.24, with a mean value $\langle c \rangle = 1.9 \pm 0.2$ (similar to 47 Tuc). It is worth mentioning that the size of NGC 1835 ($r_t \simeq 50$ pc) is quite comparable with the size of ω Centauri and 47 Tuc.

Depending on the model, the values obtained for the total mass of the cluster range from 0.70 to 1.55 $10^6\,M_\odot$, with a mean total mass $\langle M_{tot} \rangle = 1.0 \pm 0.3\ 10^6\,M_\odot$. From Table 1, we see that the best results obtained by transforming the tidal radius r_t into mass (under the assumption of systemic rotation of the old

Table 3. NGC 1835: parameters and general results about structure, density, mass and relaxation time for the 6 best King-Michie models, constrained by the composite surface brightness profile from Elson & Freeman (1985), Mateo (1987), and Meylan & Djorgovski (1990) and by the new core projected velocity dispersion

Model index	m_{hr}	x	M_{hr} %	M_{wd} %	r_a/r_c	c	r_c [pc]	r_h [pc]	r_t [pc]	ϱ_0 [$M_\odot$ pc^{-3}]	ϱ_h [$M_\odot$ pc^{-3}]	ϱ_t [$M_\odot$ pc^{-3}]	M_{tot} [$10^6\,m_\odot$]	t_{rh} [10^9 yr]	$t_{r,0}$ [10^6 yr]
(1)	(2)	(3)	(4)	(5)	(6)	(7)	(8)	(9)	(10)	(11)	(12)	(13)	(14)	(15)	(16)
1	0.0	1.25	0	19	∞	1.81	0.74	8.5	48	$2.6\ 10^4$	$2.0\ 10^2$	$2.2\ 10^0$	1.03	8.6	15.0
2	0.0	1.00	0	26	30	1.87	0.64	7.6	48	$3.4\ 10^4$	$2.2\ 10^2$	$1.8\ 10^0$	0.81	5.7	11.0
3	0.0	1.00	0	26	20	1.83	0.74	7.4	49	$2.6\ 10^4$	$2.4\ 10^2$	$1.6\ 10^0$	0.80	5.5	15.0
4	1.4	1.75	1	9	∞	1.87	0.74	11.0	55	$2.4\ 10^4$	$1.5\ 10^2$	$2.2\ 10^0$	1.55	18.0	13.0
5	1.4	1.50	2	13	30	1.94	0.59	9.1	51	$3.4\ 10^4$	$1.7\ 10^2$	$1.9\ 10^0$	1.10	10.0	7.0
6	1.4	1.25	4	18	20	2.24	0.36	7.7	64	$8.3\ 10^4$	$1.8\ 10^2$	$6.5\ 10^{-1}$	0.70	5.8	2.4
4a	1.4	1.25	4	18	∞	1.69	0.97	6.7	48	$1.8\ 10^4$	$3.1\ 10^2$	$1.7\ 10^0$	0.78	4.8	29.0
5a	1.4	1.50	2	13	30	1.94	0.59	9.1	51	$4.2\ 10^4$	$2.1\ 10^2$	$2.4\ 10^0$	1.33	11.0	7.6
5b	1.4	1.50	2	13	30	1.94	0.47	7.2	41	$5.4\ 10^4$	$2.8\ 10^2$	$3.1\ 10^0$	0.87	6.7	4.5

Table 4. NGC 1835: general results about luminosity and mass-to-light ratios for the 6 best King-Michie models, constrained by the composite surface brightness profile from Elson & Freeman (1985), Mateo (1987), and Meylan & Djorgovski (1990) and by the new core projected velocity dispersion

Model index	μ_0 [mag arcmin^{-2}]	V_t [mag]	(M/L_V) [$\odot$ units]	$(M/L_V)_0$ [$\odot$ units]
1	6.67	9.88	3.58	1.93
2	6.64	9.89	2.83	2.08
3	6.70	9.86	2.71	1.93
4	6.67	9.85	5.21	1.83
5	6.72	9.87	3.76	2.16
6	6.53	9.91	2.50	2.63
4a	6.75	9.86	2.65	1.76
5a	6.72	9.87	4.56	2.62
5b	6.72	9.87	4.74	2.72

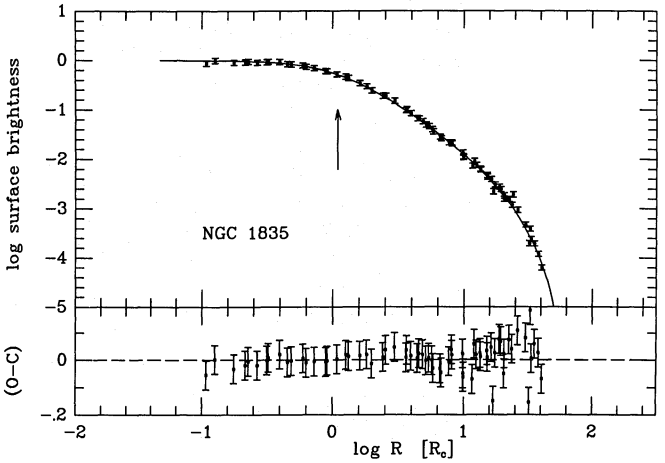

Fig. 5. NGC 1835: logarithm of the observed and projected (population 3) surface brightness profiles as a function of the logarithm of the radius (model 1 of Tables 3 and 4). The vertical arrow at 1.1 r_c corresponds to a distance of 3″ from the center and represents the sampling area over which the integrated light spectra have been obtained

Table 5. NGC 1835: mean values of the astrophysical parameters obtained in this study

Astrophysical parameter		Representative mean value
IMF exponent x	x	$= 1.00 - 1.50 - 1.75$
Core radius r_c	$\langle r_c \rangle$	$= 0.6 \pm 0.2$ pc
Tidal radius r_t	$\langle r_t \rangle$	$= 53 \pm 6$ pc
Concentration $c = \log(r_t/r_c)$	$\langle c \rangle$	$= 1.9 \pm 0.2$
Anisotropy radius r_a	r_a	$= \infty - 30 - 20\, r_c$
Central surface brightness μ_0	$\langle \mu_0 \rangle$	$= 6.66$ mag arcmin^{-2}
Integrated visual magnitude V_t	$\langle V_t \rangle$	$= 9.88$ mag
Total mass M_{tot}	$\langle M_{tot} \rangle$	$= 1.0 \pm 0.3\ 10^6\, M_\odot$
Mass-to-light ratio M/L_V	$\langle M/L_V \rangle$	$= 3.4 \pm 1.0\ (M/L_V)_\odot$
Central mass-to-light ratio $(M/L_V)_0$	$\langle (M/L_V)_0 \rangle$	$= 2.1 \pm 0.3\ (M/L_V)_\odot$

globular cluster system) are smaller than the results from King-Michie models by more than a factor of ten.

The half-mass relaxation time and the central relaxation time are of the order of 10 Gyr, and 10^7 yr, respectively, allowing a large fraction of the central parts of the cluster to have been relaxed. Both isotropic ($r_a = \infty$) and anisotropic ($r_a = 20$–$30\, r_c$) models are successfully fitted to NGC 1835 (see Table 3). A real velocity dispersion profile, instead of only the central value, would allow perhaps a better evaluation of the quantity of anisotropy.

The central surface brightness μ_0 varies from 6.53 to 6.72 mag arcmin^{-2} with a mean value $\langle \mu_0 \rangle = 6.66$ mag arcmin^{-2}. The integrated visual magnitude V_t varies from 9.85 to 9.91 mag with a mean value $\langle V_t \rangle = 9.88$ mag. This last model value is between the observed values: $V_t = 9.48$ (Chun 1978), $V_t = 9.52$ (Elson & Freeman 1985), and $V_t = 10.13$ (van den Bergh 1981). The global mass-to-light ratio M/L_V varies from 2.50 to 5.21 $(M/L_V)_\odot$, with a mean value $\langle M/L_V \rangle = 3.4 \pm 1.0$ $(M/L_V)_\odot$, whereas the central mass-to-light ratio $(M/L_V)_0$ varies from 1.93 to 2.63 $(M/L_V)_\odot$, with a mean value $\langle (M/L_V)_0 \rangle = 2.1 \pm 0.3$ $(M/L_V)_\odot$. These values of the mass-to-light ratio, higher than those from the previous studies, are mainly the direct consequences of the new central value of the projected velocity dispersion, and depend also on the mass function exponent x and on the quantity of anisotropy of the velocity dispersion. The mean values of some of the above astrophysical parameters are summarized in Table 5.

5.3. *Uncertainties*

It is worth mentioning that thermal equilibrium among the different mass classes in the central parts of the cluster appears to be one of the major assumptions of the present model (see Sect. 4.2). An old globular cluster is probably partly thermalized, but how thermalized is still unknown. Some recent observational indications of mass segregation in two galactic globular clusters, namely M71 (Richer & Fahlman 1989) and M30 (Bolte 1989), although very important, remain more qualitative than quantitative. Mass segregation has been one of the early important results to emanate from small N-body simulations. Since then, direct integrations using a few hundred stars, and models integrating the Fokker-Planck equation for many thousands of stars, have shown the same tendency. The problem of equipartition does not reside

in its hypothetical existence (it is happening), but rather in its quantitative importance, its evolution, and its end. Spitzer (1969) gives a criterion which indicates, when violated, that the large self-attraction of the heavier stars drives them into a high temperature subsystem in the core of the cluster. Underlying this is the problem of core collapse (Inagaki & Wiyanto 1984; Inagaki & Saslaw 1985; Murphy & Cohn 1988; Chernoff & Weinberg 1990).

The King-Michie model used here does not verify strict equipartition: the energy cutoff in Eq. (5) affects the lighter stars more strongly than the heavier ones, reducing their velocity dispersion. Fortunately, this is similar to the effect discribed by Inagaki & Saslaw (1985), i.e., that the different mass components are unlikely to achieve thermal equilibrium, even in the core: the central "temperature" of the heaviest and lightest stars differ by a factor of ~ 2, the largest differences occurring for models with low x values of the IMF exponent (i.e., with many high mass stars).

The degree of thermalization in NGC 1835 remains observationally unknown. In order to investigate the sensitivity of the present results to this major assumption (assumption suggested by both theoretical arguments and numerical simulations), some models are calculated with only partial thermalization, i.e., with $A_i \propto \bar{m}_i^{1/2}$ instead of $A_i \propto \bar{m}_i$. One of these successfully fitted models, with index 4a, is given in Tables 3, and 4. Compared with model 4 (the most similar from a parameter point of view), the most important difference concerns of course the total mass, which decreases by 50% (from $M_{\rm tot} = 1.55\ 10^6\ M_\odot$ to $M_{\rm tot} = 0.78\ 10^6\ M_\odot$).

In order to avoid sampling over a few bright stars, the integrated light spectra have been obtained over a square of $6'' \times 6''$ centered on the core, but not covering only the centermost regions (see the vertical arrow in Fig. 5, which gives the limit of the sampling area). The deduced value of the projected velocity dispersion represents a mean value, over a region of the cluster which is slightly larger than the isothermal core, and thus could be underestimated. The consequences of such an observational bias can be investigated by computing a few models. The central projected velocity dispersion taken equal to 11.1 km s^{-1} instead of 10.1 km s^{-1}, all the other parameters being similar, gives the results displayed in Tables 3 and 4 for the model with index 5a. The total mass is increased by about 20% (from $M_{\rm tot} = 1.10\ 10^6\ M_\odot$ to $M_{\rm tot} = 1.33\ 10^6\ M_\odot$, for models 5 and 5a, respectively) with the corresponding consequences on the spatial stellar densities, relaxation times and mass-to-light ratios.

The distance modulus taken equal to 18.2 instead of 18.7 (e.g., Anderson et al. 1985), all the other parameters being similar, gives the results displayed in Tables 4 and 5 for the model with index 5b. The total mass is decreased by about 20% (from $M_{\rm tot} = 1.10\ 10^6\ M_\odot$ to $M_{\rm tot} = 0.87\ 10^6\ M_\odot$, for models 5 and 5b, respectively), with the corresponding consequences on the linear dimensions of the cluster (r_c, r_h, and r_t), on its spatial stellar densities, relaxation times and mass-to-light ratios.

6. A universal M/L_V ratio for old globular clusters?

The projected velocity dispersion in the core of the old Large Magellanic Cloud globular cluster NGC 1835 is deduced from integrated light spectra obtained at the European Southern Observatory (ESO) with CASPEC, the Cassegrain ESO Echelle Spectrograph mounted on the ESO 3.6-m telescope at La Silla, Chile. Numerical cross-correlation technique gives a projected velocity dispersion value σ_p (core) $= 10.1 \pm 0.2$ km s^{-1}.

A multi-mass anisotropic dynamical (King-Michie) model, based on an assumed form of the phase-space distribution function $f(E, J)$, allows the investigation of the internal structure of NGC 1835.

The total mass of the cluster, depending on the model, ranges from 0.70 to $1.55\ 10^6\ M_\odot$, with a mean total mass $\langle M_{\rm tot} \rangle = 1.0 \pm 0.3\ 10^6\ M_\odot$. The global mass-to-light ratio M/L_V varies from 2.50 to 5.21 $(M/L_V)_\odot$, with a mean value $\langle M/L_V \rangle = 3.4 \pm 1.0\ (M/L_V)_\odot$, whereas the central mass-to-light ratio $(M/L_V)_0$ varies from 1.93 to 2.63 $(M/L_V)_\odot$, with a mean value $\langle (M/L_V)_0 \rangle = 2.1 \pm 0.3\ (M/L_V)_\odot$.

The present results concerning the total mass of NGC 1835 are larger than the best previous determinations (not using King-Michie models) by about a factor of ten, giving this old LMC globular cluster a M/L_V ratio similar to those obtained for galactic globular clusters (Table 1). Consequently, the method based on the assumption of circular orbit of the clusters in rotation around the center of mass of the LMC and on the transformation of the tidal radius into mass should be used only with great care in the case of Magellanic clusters. The systematic difference observed between the typical mass of rich globular clusters in the Galaxy (greater than $10^5\ M_\odot$) and in the Magellanic clouds (less than $10^5\ M_\odot$) could be a simple artifact, a direct consequence of the idiosyncrasies of the different methods used.

In conclusion, when the same kind of dynamical models (King-Michie) constrained by the same kind of observations (surface brightness profile and central value of the velocity dispersion) are applied to an old rich Magellanic globular cluster, viz., NGC 1835, the results seem similar to those obtained in the case of 47 Tucanae. Consequently, the rich old globular clusters in the Magellanic clouds could be quite similar (in mass and M/L_V) to the rich globular clusters in the Galaxy.

Acknowledgements. We would like to thank the European Southern Observatory for allocation of a few hours of observing time during a test night, which allowed us to investigate the applicability of the present version of numerical cross-correlation technique. The Swiss National Science Foundation is acknowledged for partial financial support.

References

Andersen, J., Blecha, A., Walker, M.F., 1985, A & A, 150, L12
Baranne, A., Mayor, M., Poncet, J.L., 1979, Vis. Astron. 23, 279
Benz, W., Mayor, M., 1981, A & A 93, 235
Benz, W., Mayor, M., 1984, A & A 138, 183
Bolte, M., 1989, AJ 341, 168
Chernoff, D.F., Weinberg, M.D., 1990, ApJ 351, 121
Chun, M.S., 1978, AJ 83, 1062
de Medeiros, J.R., Mayor, M., 1990, Sixth Cambridge Workshop on Cool Stars, Stellar System, and the Sun, Seattle, September 11–14, 1989, in Astronomical Society of the Pacific's Conference Series, Vol. 9, ed. G. Wallerstein, p. 404
de Vaucouleurs, G., Freeman, K.C., 1973, Vis. Astron. 16, 163
Elson, R.A.W., Freeman, K.C., 1985, ApJ 288, 521
Feitzinger, J.V., 1980, Space Sci. Rev. 27, 35
Freeman, K.C., 1974, ESO/SRC/CERN Conference on Research Prog. for the New Large Telesc. Geneva, p. 177
Freeman, K.C., 1980, Star Clusters IAU Symp. 85, Victoria 1979, ed. J.E. Hesser, p. 317
Freeman, K.C., Illingworth, G., Oemler, A., 1983, ApJ 272, 488

Griffin, R.F., 1967, ApJ 148, 465
Griffin, R.F., 1968, A Photometric Atlas of the Spectrum of Arcturus Cambridge, Phil. Soc.
Gunn, J.E., Griffin, R.F., 1979, AJ 84, 752
Guseinov, O.H., Novruzova, H.I., Rustamov, Yu.S., 1983, Ap & SS 97, 305
Harris, W.E., 1987, PASP 99, 1031
Iben, I., Renzini, A., 1983, ARA & A, ed. G. Burbidge, vol. 21, p. 298
Illingworth, G.D., 1973, Ph.D. thesis, Mount Stromlo Observatory, Australia
Illingworth, G.D., 1976, ApJ 204, 73
Inagaki, S., Wiyanto, P., 1984, PASJ 36, 391
Inagaki, S., Saslaw, W.C., 1985, ApJ 292, 339
King, I.R., 1962, AJ 67, 471
King, I.R., 1966, AJ 71, 64
Kontizas, M., 1984, A & A 131, 58
Kontizas, M., 1986, A & AS 65, 207
Latham, D.W., 1985, Stellar Radial Velocities IAU Coll. 88, Schenectady, 1984, ed. A.G. Davis Philip, Davis Press, Schenectady, p. 21
Lightman, A.P., Shapiro, S.L., 1978, Rev. Modern Phys. 50, 437
Lupton, R., Gunn, J.E., Griffin, R.F., 1985, Dynamics of Stars Clusters IAU Symp. 113, Princeton 1984, eds. J. Goodman, P. Hut, p. 19
Lupton, R., Gunn, J.E., Griffin, R.F., 1987, AJ 93, 1114
Mateo, M., 1987, Ph.D. Thesis, University of Washington
Meylan, G., 1987, A & A 184, 144
Meylan, G., 1988a, A & A 191, 215
Meylan, G., 1988b, ApJ 331, 718
Meylan, G., 1989, A & A 214, 106
Meylan, G., Djorgovski, S., 1990, ApJ (in preparation)
Meylan, G., Mayor, M., 1988, BAAS 20, 963
Meylan, G., Mayor, M., 1990, A & A (in preparation)
Michie, R.W., 1963, MNRAS 126, 499
Murphy, B.W., Cohn, H.N., 1988, MNRAS 232, 835
Peterson, R.C., Seitzer, P., Cudworth, K.M., 1989, AJ 347, 251
Prévot, L., Rousseau, J., Martin, N., 1989, A & A 225, 303
Pryor, C., McClure, R.D., Fletcher, J.M., Hartwick, F.D.A., Kormendy, J., 1986, AJ 91, 546
Pryor, C., McClure, R.D., Fletcher, J.M., Hesser, J.E., 1989, AJ 98, 596
Pryor, C., McClure, R.D., Fletcher, J.M., Hesser, J.E., 1990, AJ (in press)
Renzini, A., Buzzoni, A., 1986, Spectral Evolution of Galaxies Fourth Workshop of the Advanced School of Astronomy, Erice, 1985, eds. C. Chiosi, A. Renzini, p. 195
Richer, H.B., Fahlman, G.G., 1989, ApJ 339, 178
Salpeter, E.E., 1955, ApJ 121, 161
Seitzer, P., 1988, Progress and Opportunities in Southern Hemisphere Optical Astronomy A.S.P Conf. Series No. 1, eds. V.M. Blanco, M.M. Phillips, p. 389
Seitzer, P., 1990, ApJ (in preparation)
Spitzer, L., 1969, ApJ 158, L139
Spitzer, L., Hart, M.H., 1971, ApJ 164, 399
van den Bergh, S., 1981, A & AS 46, 79
Weidemann, V., 1987, A & A 188, 74
Weidemann, V., Koester, D., 1983, A & A 121, 77